Sustainable Energy & Fuels

ROYAL SOCIETY OF CHEMISTRY

PAPER

View Article Online
View Journal | View Issue

Cite this: *Sustainable Energy Fuels*, 2023, 7, 4567

Overcoming residual carbon-induced recombination in water-oxidation catalysis: combining a superior catalyst with low-carbon-content atomic layer deposition of SnO_2 for improved catalysis†

Carly F. Jewell, [a] Ashwanth Subramanian, [b] Won-Il Lee,[b] Chang-Yong Nam *[cb] and Richard G. Finke *[a]

Received 20th February 2023
Accepted 28th July 2023

DOI: 10.1039/d3se00222e

rsc.li/sustainable-energy

Previously an all earth-abundant dye-sensitized photoelectrochemical cell, composed of nanostructured SnO_2 coated in perylene diimide dye (*N*,*N*′-bis(phosphonomethyl)-3,4,9,10-perylenediimide, PMPDI) plus photoelectrochemically deposited cobalt oxide (CoO_x) catalyst, was shown to photoelectrochemically oxidize water. However, in that earlier work and device the addition of a known water-oxidation catalyst (WOCatalyst), CoO_x, was found to *reduce* photocurrents, an effect that we termed an "anti-catalyst" effect to emphasize its unexpected, opposite-from-desired nature. The cause of the anti-catalyst effect was discovered to be residual carbon in the nanostructured SnO_2 scaffolding necessary to increase surface area and photocurrents, hence actually *residual-C-containing* SnO_xC_y scaffolding. Herein, we examine two approaches to overcome this undesired anti-catalyst effect. First, we demonstrate photocurrent improvement with the addition of a more active, state-of-the-art, amorphous Li-IrO_x, WOCatalyst. Second, we employ more phase-pure, planar SnO_2 prepared by atomic layer deposition (ALD) and quantitatively compare, by optical absorption and double-layer capacitance measurements, the performance of ALD-SnO_2 *vs.* the nano-SnO_xC_y made in house following a literature recipe. The more phase-pure ALD-SnO_2 yielded higher photocurrents based on either per dye or per electrochemically active surface area basis. Finally, in a third approach we combine both strategies for overcoming the anti-catalyst effect, specifically we use the best-in-class Li-IrO_x catalyst *and* ALD-SnO_2 to generate a best-performing device to date for this system. The results offer three successful approaches to overcome the anti-catalyst effect caused by residual-carbon-based recombination.

Introduction

Rising global demand for renewable energy has led to increased interest in and research on storable solar energy, particularly though the use of photocatalytic conversion of water into oxygen and hydrogen.[1–5] A dye-sensitized photoelectrolysis cell (DS-PEC) designed to anodically split water generally requires a minimum of three components: a molecular light absorbing complex such as a dye, a semiconductor for charge transport, and a catalyst facilitating the oxidation of water.[1,6,7] Organic dyes have drawn particular interest in recent years as light absorbers for solar-based water splitting as they are relatively cheap, can be made using all earth-abundant elements, and are synthetically highly tunable.[1,8–10] The use of earth-abundant materials in water-oxidation catalysis (WOC) systems is desirable for sustainable, long-term use. Hence, significant work has been done researching WOC systems comprised of earth-abundant elements.[11–14]

However, WOC is a complex kinetics system with many opportunities for inefficiency due to recombination. Prioritizing more plentiful elements over more efficient, but rarer-element, catalysts often introduces further inefficiencies. As a result, dye-sensitized water oxidation anodes made of all earth-abundant materials are less frequently reported, and those that have been reported are still not competitive with rare-element-based catalysts (Table 1). For example, a recently reported, all earth-abundant anode comprising a Prussian blue analog used with a Janus green B dye on rutile TiO_2 resulted in photocurrents of 50 μA cm^{-2} at +0.8 V *vs.* NHE (normal hydrogen electrode), but

[a]*Department of Chemistry, Colorado State University, Fort Collins, Colorado, 80523, USA. E-mail: Richard.Finke@colostate.edu; cynam@bnl.gov*

[b]*Department of Materials Science and Chemical Engineering, Stony Brook University, Stony Brook, New York, 11794, USA*

[c]*Center for Functional Nanomaterials, Brookhaven National Laboratory, Upton, New York, New York 11973, USA*

† Electronic supplementary information (ESI) available: Details on the determination of the electrochemically-active surface area and the deposition of Li-IrO_x. See DOI: https://doi.org/10.1039/d3se00222e

Table 1 Relative photocurrents for selected DS-PEC water oxidation systems using both earth-abundant and non-earth abundant catalysts

Paper	Water oxidation catalyst	Dye	Scaffolding	Photocurrent	Light source	All earth-abundant system?
Finke and coworkers, 2017 [12]	CoO_x	PMPDI	Nano-SnO_2	20 μA cm^{-2} at +0.4 V *vs.* NHE, pH 7	AM 1.5G	Yes
Karadas and coworkers, 2020 [15]	Prussian blue analog	Janus green B	Rutile TiO_2	50 μA cm^{-2} at +0.8 V *vs.* NHE, pH 7	100 mW cm^2, λ > 420 nm	Yes
Meyer and coworkers, 2022 [32]	CoF, Co_4O_4 cubic complex	D–π–A[a]a	TiO_2	120 μA cm^2 at +0.6 V *vs.* NHE), pH 7	100 mW cm^2, λ > 400 nm	Yes
Bignozzi and coworkers, 2015 [24]	IrO_2	Perylene bisimide	WO_3	70 μA cm^{-2} at +0.30 V *vs.* NHE, pH 3	AM 1.5G, λ > 450 nm	No
Sun and coworkers, 2015 [20]	Ru-pdc[c]	D–A[d]	TiO_2	300 μA cm^{-2} at +0.36 V *vs.* NHE, pH 7	100 mW cm^2, λ > 400 nm	No
Meyer and coworkers, 2017 [30]	Ru(bda)[b]	D–π–A[a]a	TiO_2/Al_2O_3 core–shell	400 μA cm^{-2} at +0.4 V *vs.* NHE, pH 4.8	100 mW cm^2, λ > 400 nm	No
Bonchio and coworkers, 2022 [31]	Ru_4POM[e]	PBI QS-TEG_{lock}[f]	Inverse opal-ITO	370 ± 30 μA cm^{-2} at +1.52 V *vs.* RHE, pH 7	AM 1.5G, 850 mW cm^2, λ > 450 nm	No

[a] Donor–π–acceptor dye. [b] Ru(bda)-$(pyP)_2$ (bda is 2,2′-bipyridine-6,6′-dicarboxylate; pyP is (3-(pyridin-4-yloxy)propyl)phosphonic acid). [c] Ru-(pdc)(pic)3 with pyridine-2,6-dicarboxylic acid (pdc) as an anchoring group, pic = 4-picoline. [d] Donor–acceptor dye, 4-(diphenylamino)phenyl cyanoacrylic acid. [e] $Ru_4(\mu\text{-}O)_4(\mu\text{-}OH)_2(H_2O)_4(\gamma SiW_{10}O_{36})_2]^{10-}$. [f] Bis-cationic perylenebisimides quantasomes interlocked with tetraethylene glycol.

exhibited charge recombination issues attributable to competitive charge recombination reactions and inefficient injection of the excited electrons.[15]

Dye-sensitized water-oxidizing photoanodes using rare-metal catalyst are much more common in the literature and achieve much higher photocurrents. Many current, state-of-the-art water oxidation catalysts (WOCatalysts) are made of more expensive metals such as ruthenium[16–21] and iridium.[22–29] Anodes using Ru-based catalysts have achieved photocurrents on the order of 400 μA cm^{-2} at +0.4 V *vs.* NHE,[30] 370 ± 30 μA cm^{-2} at +1.52 V *vs.* RHE,[31] and 300 μA cm^{-2} at +0.36 V *vs.* NHE.[20] On the basis of the literature, a rare-element-based Ir catalyst was chosen for the research herein in order to optimize photocurrents while addressing the specific questions posed, *vide infra*.

Previously, our group developed a water-oxidation system consisting of all earth-abundant materials: nano-SnO_xC_y coated with a perylene diimide dye, *N*,*N*′-bis(phosphonomethyl)-3,4,9,10-perylenediimide (PMPDI), and CoO_x as a WOCatalyst.[12,13] Although the materials in this system are generally more environmentally friendly than typical Ru or Ir-based catalysts, the addition of the CoO_x catalyst resulted in an, at the time unexpected, undesired *decrease* in photocurrent that we termed an "anti-catalyst" effect.[12,13] Tracking down the origins of this "anti-catalyst" effect eventually led to the discover that this undesired behavior is attributable to carbon impurities in the SnO_2, that is, to residual carbon in the nano-SnO_xC_y.[33] Research by other groups found they, too, can alter the photoelectrochemistry of a SnO_2 system by changing the carbon in the system.[34] Interestingly, an *increase* in photocurrent density was observed in Sn–C systems, which was attributed to the formation of a heterostructure with decreased resistance,[34] a reversal in trend from the observed effect in the system detailed in this paper.[33]

Herein, we pose and experimentally address the following five questions: (1) Can improving the WOCatalyst in the system overcome and outcompete such recombination pathways? That is, can a more active WOCatalyst impact the primary charge-transfer pathways during water oxidation by altering its kinetics, an important question with implications for optimizing the WOC in the present device and potentially other WOC devices moving forward. Note here that the cost of initially more expensive catalysts can prove to tend towards zero if their catalytic lifetimes tend toward "infinity", that is reach high numbers of total turnovers of catalysis. Then, (2) what is *the maximum current* from such an improved device? Benchmarking that maximum current is important as one strives to prepare improved, future earth-abundant WOCs devices. Additionally, (3) can we utilize atomic-layer deposition (ALD) of planar SnO_2 as an effective way[33] to address the residual carbon in the nano-SnO_xC_y scaffolding, that is, as a way to reduce the residual C in the nano-SnO_xC_y, ideally sufficiently to produce a positive catalytic effect following CoO_x addition?[33] To this end, we will compare the performance of the lower-surface-area planar ALD-SnO_2 device to its high-surface-area nano-SnO_xC_y counterpart by developing a way to correct for the very different surface areas of the two systems while answering the question:

(4) is an intrinsic improvement in photocatalytic efficiency achieved in the planar system with its low-C-content SnO_2?; (5) Finally, can we achieve and quantify a further improved WOC device by *combining* the best-performing ALD-SnO_2 and a best-in-class WOCatalyst, Li-IrO_x? Overall, this research strives to provide quantitative insights into the ways one can test new materials for complex WOC anodes en route to ensuring that the device components are not limited by catalyst choice. Our results also illustrate how and why testing both earth-abundant and precious metal catalysts can be used to address charge recombination issues and to set a benchmark for the maximum current available from a given device.

Experimental

Experimental conditions used herein are identical to those in our previously published work,[11–13,33] unless otherwise noted. Key experimental details are provided below and in the ESI† as necessary to ensure that the present manuscript is largely self-contained and replicable by others.

Materials

The following starting materials and solvents were used as received to generate buffer solutions: KOH (Fisher, Certified ACS grade, 98.5%, 1.5% water, 0.00028% Fe, 0.0008% Ni); KH_2PO_4 (Fisher, Certified ACS Grade, 99.3%, 0.0005% Fe); ethanol (Pharmco-Aaper, ACS grade); hydroquinone (Aldrich, >99%); NANOpure water (Barnstead NANOpure ultrapure water system, 18.0 MΩ). NANOpure water was used for all experiments.

Synthesis of Li-IrO_x

Using the synthesis procedure reported by Gao *et al.*,[35] Li-IrO_x was synthesized as detailed in Scheme 1. Briefly, 250 mg of iridium(III) chloride hydrate (Aldrich, reagent grade) was dissolved into 5 mL of water. Then, 5.0 g of $LiOH \cdot H_2O$ (Sigma; 150 equivalents *vs.* Ir) was added. This solution was then heated to 90 °C with stirring in order to remove the water by evaporation. The solid remaining was then placed in a crucible and heated to 400 °C for 2 hours under air. After cooling, the resultant solid Li-IrO_x product was rinsed three times with water and ethanol then dried at 60 °C overnight at 1 atm. The final Li-IrO_x product was found to be comparable to the previously published material by X-ray photoelectron spectroscopy (XPS), detailed below and in the ESI.†[35]

Planar SnO_2 preparation by ALD

As before,[33] ultrathin conformal coatings of SnO_x were carried out using the Cambridge Nanotech Savannah S100 ALD system (base pressure of ~0.43 Torr) at a temperature of 85 °C. SnO_x depositions were done using sequential exposures to tetrakis(dimethylamido)tin(IV) (TDMASn) (Strem Chemicals) (200 ms) and water vapor (15 ms) with an intermediate purge time of 10 s for both the precursors.

Preparation of nano-SnO_xC_y/PMPDI anodes

Nano-SnO_xC_y was prepared as before using a modified literature procedure[36] previously optimized for the present system.[12,33] Briefly, 800 mg of white commercially available SnO_2 nanopowder (SnO_2, NanoArc©, Alpha Aesar, Lot Analysis: 99.6% SnO_2, 47 $m^2\ g^{-1}$ specific surface area by BET (Brunauer–Emmett–Teller) method, 18 nm average particle size, 6.95 g cm^{-3} density) was massed into a 20 mL scintillation vial to which a Teflon-coated magnetic stir bar was added. The powder was then wetted with 1.0 mL of glacial acetic acid (ACS grade, Mallinckrodt), stirred until fully mixed, and then placed into an ultrasonic water bath (Branson 2510) for 5 min. Next, 4.0 mL of water was added to the paste and the resulting mixture was stirred for 5 min on a stir plate. The paste was then sonicated twice using a QSonica Q125 ultrasonic liquid microprocessor (1/8″ probe), which was held at 80% amplitude. To this mixture, 1.10 g of polyethyleneglycol bisphenol A epichlorohydrin copolymer (PEG-BAE) (Sigma, M_w = 15 000–20 000), which serves as a thickening agent, was added in individual small chunks while stirring. After all the PEG-BAE had been added and dissolved fully upon visual inspection, one drop (approximately 20 mg) of Triton X-100 (octyl phenoxy polyethoxyethanol, Sigma) was added using a plastic transfer pipet in order to increase adhesion of the paste to the glass substrate. This final paste was then stirred overnight and then refrigerated in a sealed vial. All synthetic and manufacturing details for PMPDI dye can be found in our previous publications.[11,12] In order to manufacture the nano-SnO_2 anodes, the previously described nano-SnO_2 paste was doctor bladed onto fluorine-doped tin oxide (FTO)-coated glass using a 2-Scotch thickness and annealed under air for 1 hour at 450 °C.[12] The PMPDI dye was loaded onto the FTO coated in either nano-SnO_2 or ALD-SnO_2 anodes for 24 hours at 95 °C from a saturated solution of fully protonated PMPDI in water.[12]

Deposition of Li-IrO_x onto nano-SnO_xC_y/PMPDI anodes

Li-IrO_x catalyst (2.5 mg), prepared as above, was dissolved into 1.0 mL of a 95 : 5 v/v ethanol: water mixture. Previous work

$$1\ IrCl_3{\bullet}H_2O_{(s)} + 150\ LiOH{\bullet}H_2O_{(s)} \xrightarrow[\text{Heat to 400 °C for 2 h}]{\substack{5.0\ mL\ H_2O_{(l)} \\ \text{Heat to 90 °C until dry}}} Li_y\text{-}IrO_{x(s)} + 3\ LiCl_{(aq)} + 147\text{-}y\ LiOH_{(s)} + H_2O_{(l)}$$
$$\text{Wash with EtOH and } H_2O$$

Scheme 1 Literature-based synthesis of Li-IrO_x following Gao and coworkers experimental.[35]

using the Li-IrO_x catalyst deposited the Li-IrO_x using a "custom external-mixing two-fluid nozzle".[29] *In lieu* of this unavailable custom-made device, a handheld nebulizer (Hudson RCI, Micro Mist) was used with air to spray droplets of the Li-IrO_x solution onto the anode. Air pressure was set to the minimum value sufficient to nebulize the solution. Care was taken to ensure the mixture deposited uniformly onto the anode by using a modified nebulizer to narrow the size of the spray equal to the anode size. Further information on the nebulizing device can be found in ESI S3.† The resulting anode was then annealed at 120 °C for 10 min under air.

Deposition of CoO_x

CoO_x WOCatalyst was added to photoanodes by photoelectrochemical deposition.[11,12] The FTO/SnO_2/PMPDI anodes were placed into a solution of pH 7, 0.5 mM $Co(NO_3)_2$ and 0.1 M potassium phosphate buffer (KPi) and held at +0.2 V *vs.* Ag/AgCl under 1 sun illumination for 3 min.[12] Anodes were then rinsed with water for 30 s and allowed to air dry. Note the same charge was observed to be passed on both planar and nanostructured SnO_2 anodes.

Photoelectrochemical testing

All photoelectrochemical experiments were done in a previously described[11–13] custom two-compartment Pyrex cell. The custom cell has two compartments separated by a medium porosity glass frit: a working compartment ($1 \times 1.5 \times 1.5$ cm^3, 5 mL) and an auxiliary compartment. A CH Instruments CHI-750D bipotentiostat, a Pt wire counter electrode, and a Ag/AgCl (3 M NaCl, +0.215 V *vs.* NHE) reference electrode were used for all experiments. The counter electrode was placed alone in the auxiliary compartment to separate the products from the working and counter electrodes. The reference electrode was positioned in the working compartment near the working electrode anode's surface in order to minimize resistance. The anode of interest was held with an alligator clip to the front wall of the working compartment with the undyed, nonconductive glass side pressed flat against the compartment wall nearest the incoming light. Both sides of the cell were filled with *ca.* 5 mL of electrolyte (pH 7, 0.1 M KPi buffer), an amount sufficient to cover the dyed film. The anode was illuminated using a 65 W xenon arc lamp (PTO model A1010), powered using an OLIS XL150 adjustable power supply. The light from the xenon arc lamp was passed through both a bandpass filter (315–710 nm, Thorlabs KG3, FGS900S) and an ultraviolet filter (400 nm long-pass, Thorlabs FGL400S) before reaching the anode. The power density of the light was adjusted to match the visible region of the airmass 1.5 global (AM 1.5G) spectrum.[12] In experiments with transients (interrupted illumination) a manual shutter was used to block the light.[12] Each anode was tested with a series of electrochemical experiments in the order detailed below: (1) the cell was allowed to short-circuit in the dark for 60 s to depopulate the electrons from SnO_2 sub-bandgap states.[12] (2) The open-circuit potential, V_{oc}, of the anode was measured *vs.* the Ag/AgCl reference electrode for 90 s both in the dark and (3) again under illumination. (4) A photocurrent transient experiment in which the anode was held at +0.2 V *vs.* Ag/AgCl for 300 s with 30 s light/dark transients throughout was next conducted. (5) The anode was then allowed to short-circuit again in the dark for 60 s, and the V_{oc} in both the (6) dark and (7) light were remeasured for 90 s each. (8) A current–voltage (*i*–*V*) photocurrent transient experiment was performed where the voltage was scanned from −0.2 V to +1.0 V *vs.* Ag/AgCl using a 10 mV s^{-1} scan rate and 5 s light transients. For each experiment and each set of conditions being tested, every experiment was reproduced a minimum of three times with three separate anodes prepared under identical conditions. All figures and values reported herein are representative examples of the photoactivity of the anode system indicated. Care was taken to ensure that the reported results are reproducible and are not due to a defective anode or otherwise irreproducible sample.

XPS

XPS was done in house using a PE-5800 series Multi-Technique ESCA XPS system. An Al Kα monochromatic source operating at 350.0 W was used for all XPS experiments. High-resolution (HRES) scans were carried out for all elements present (carbon, lithium, oxygen, iridium) in the initial survey scan at a minimum of 3 spots across the sample surface for 30 min apiece. To fit the data, CASAXPS software was used to analyze the data. Quantification results for each element were tabulated using an average of each replicate scan. Consistent with both the literature method of XPS fitting and ensuring self-consistency across fits, HRES spectra were calibrated to a 285 eV aliphatic carbon peak.[37,38] Fits were done using a minimum, Ockham's Razor type approach to ensure the data was not overfit (Fig. S1†).

Oxygen detection

Oxygen yield was measured using the generator–collector (G–C) technique detailed previously.[12,13,39–41] Photoanodes of interest, "generators", were placed with conductive sides facing the conductive side of a FTO "collector".[12] The generator and collector were then separated by a Parafilm spacer. The G–C device was placed in the working compartment detailed above, with the generator side flush against the wall of the cell nearest the incoming light. The cell was filled with approximately 10 mL pH 7, 0.1 M KPi buffer, sufficient to fully cover the dyed portion of the anode, which was degassed with Ar for a minimum of 60 min to remove oxygen. Current was measured at both the generator and collector electrodes, which were held at +0.2 V and −0.65 V *vs.* Ag/AgCl, respectively. The current was collected for 300 s in the dark to obtain a background, 300 s in the light to generate oxygen, then 300 s in the dark to ensure all oxygen fully diffused between the two electrodes and that all current attributable to oxygen production was collected. Control experiments with FTO/CoO_x anodes were used to determine the collection efficiency of the G–C device[12] and used to calculate the O_2 yield and faradaic efficiency of each photoanode.

Results and discussion

As a test of our first specific question, of how a different WOCatalyst can impact primary charge transfer and possibly overcome recombination due to carbon defects,[33] a known state-of-the-art WOCatalyst, amorphous Li-IrO_x,[29,35] was added our otherwise earth-abundant nano-SnO_xC_y/PMPDI DS-PEC water-oxidation catalysis system. The addition of the Li-IrO_x allows us to continue to use the increased surface area provided by nanostructuring the device with nano-SnO_xC_y, but seeks to kinetically outcompete recombination attributed to carbon in the nano-SnO_xC_y as judged to start by an increase in photocurrent.[33] Additionally, the highest photocurrent one can observe for the nano-SnO_xC_y/PMPDI/**Li-IrO_x** anode sets a benchmark for photocurrents one can strive for *via* the future development of improved, ideally all earth-abundant, catalysts.

Addition of Li-IrO_x WOCatalyst

Li-IrO_x was synthesized as detailed in the Experimental section and deposited onto the nano-SnO_xC_y/PMPDI, resulting in nano-SnO_xC_y/PMPDI/Li-IrO_x anodes. The photoactivity of these anodes was then examined in pH 7 buffer with the addition of hydroquinone (H_2Q). As before,[11,12] H_2Q was employed as a sacrificial reductant as it exhibits a kinetically facile, $2e^-$ and $2H^+$, oxidation.[1,12,21] Photocurrent transients were carried out on the nano-SnO_xC_y/PMPDI anodes with and without Li-IrO_x catalyst in the presence of H_2Q (Fig. 1). These results were also compared to our previously published and optimized nano-SnO_xC_y/PMPDI/**CoO_x**[12] to best understand how changing the catalyst impacts photoactivity and to attempt to answer the first question posed herein seeking to understand how changing the catalyst can impact the charge-transfer kinetics of the device.[42] It is important to note here that catalyst loading was not optimized for the nano-SnO_xC_y/PMPDI/Li-IrO_x anodes demonstrating again how much more effective the Li-IrO_x is as a WOCatalyst compared to even the *optimized* CoO_x. Optimizing catalyst loading is certainly also possible, but will only exaggerate (*i.e.*, but not change the general trend of) the enhanced-current findings herein with the Li-IrO_x catalyst.

Importantly, steady-state photocurrents *increased* 10% with the addition of Li-IrO_x, *the first time we have observed an increase in the nano-SnO_xC_y containing anodes*.[12,13] This increase in photocurrent in a net improvement of 34% from the anode with the CoO_x catalyst to the Li-IrO_x catalyst. As reported previously, anodes with CoO_x WOCatalyst addition yield a *decrease* in steady-state photocurrents of 24% upon catalyst addition.[33] Hence, by changing the catalyst used with the nano-SnO_xC_y/PMPDI anodes from CoO_x to Li-IrO_x, the anti-catalyst effect is reversed and now the photocurrents *increase* to -1.2 mA cm^{-2} rather than decrease[43] with catalyst addition. Two times the -1.2 mA cm^{-2} photocurrent observed for the Li-IrO_x-containing system oxidizing H_2Q, that is -2.4 mA cm^{-2}, serves as an experimentally based, *estimated theoretical maximum* photocurrent achievable for water oxidation with this device. Also noteworthy is the *significantly lower photocurrent decay* over the course of the 30 s light transients for anodes with deposited Li-IrO_x, suggestive of facile electron-delivery-kinetics protection of the oxidized PMPDI dye.

To ensure the effect of Li-IrO_x addition in H_2Q is reflective of the true WOC performance, anodes with and without catalyst were examined in pH 7, 0.1 M KPi buffer under actual WOC conditions (*i.e.*, without any added sacrificial reductant), Fig. 2. As in the system with H_2Q, the addition of the Li-IrO_x catalyst to nano-SnO_xC_y/PMPDI anodes in the buffered water system again *increases* the system's photocurrent, contrary to what is observed for the nano-SnO_xC_y plus the less able CoO_x catalyst anodes.[12,13] With the addition of Li-IrO_x, the steady-state photocurrent of anodes increases by 50% – an increase greater than seen for the anodes tested with H_2Q. Upon reflection, this larger increase in photocurrent post catalyst addition makes sense: the $2\ e^-/2H^+$ reaction with H_2Q is kinetically much more facile than the more difficult, $4\ e^-/4H^+$, oxidation of water. Hence, an inherently higher probability of recombination in the slower, more difficult, overall $4\ e^-/4H^+$, water oxidation reaction is expected, corresponding to a greater effect of overcoming

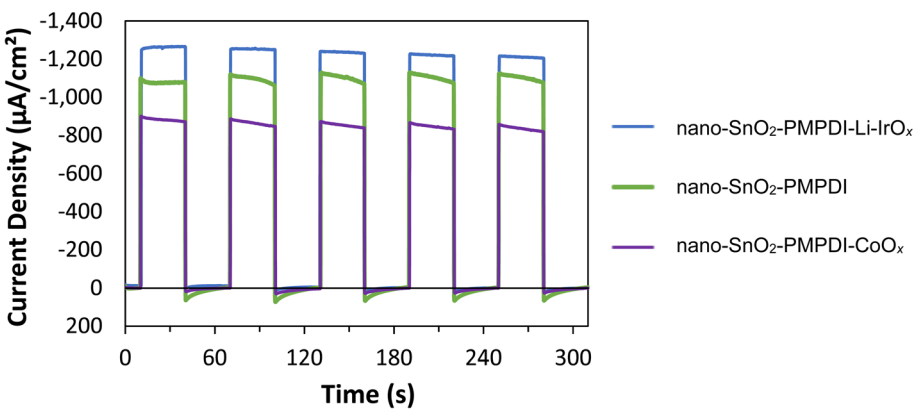

Fig. 1 Photocurrent transients in the presence of 20 mM H_2Q sacrificial reductant, with background dark current subtracted, at +0.2 V *vs.* Ag/AgCl in pH 7, 0.1 M KPi buffer with 30 s light/dark transients where blue is nano-SnO_xC_y/PMPDI/Li-IrO_x, green is nano-SnO_xC_y/PMPDI, and purple is nano-SnO_xC_y/PMPDI/CoO_x. Note here that each transient shown represents a minimum of three replicates of separately generated and tested anodes.

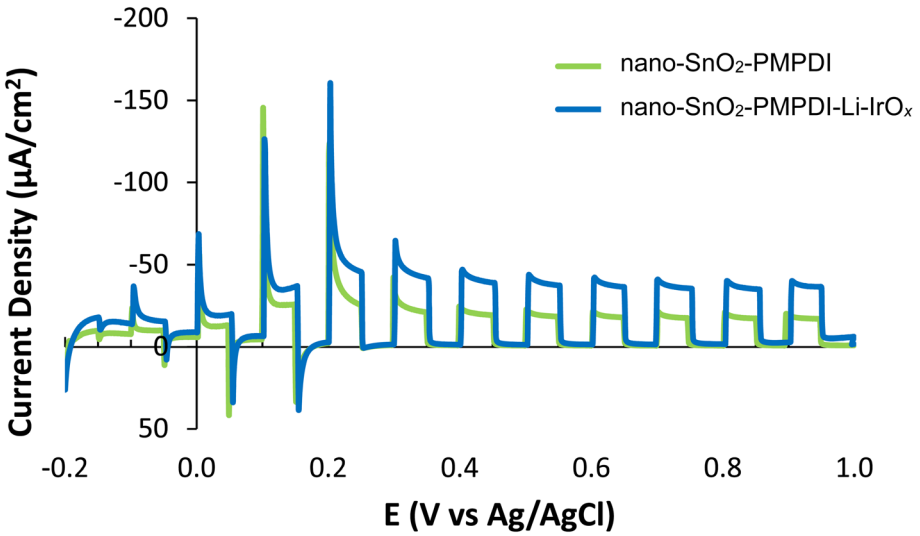

Fig. 2 Photocurrent transients for nano-SnO_xC_y/PMPDI (green) and nano-SnO_xC_y/PMPDI/Li-IrO_x (blue) anodes in pH 7, 0.1 M KPi buffer. Scans were done from −0.2 to +1.0 V *vs.* Ag/AgCl with 5 s light dark transients.

such recombination on the H_2O oxidation system *vs.* the H_2Q, hydroquinone, system.

Understanding recombination with different WOCatalysts

To provide additional evidence that this increase in photocurrent corresponds with a decrease in recombination, the V_{oc} of the anode under illumination was measured.[12,13,44] In this system, the V_{oc} can be directly related to recombination as the V_{oc} signifies the quasi-Fermi energy of electrons ($E_{F,n}$) in the nano-SnO_xC_y, with respect to the Ag/AgCl reference electrode potential.[12,13,44,45] The V_{oc} is determined by the steady-state charge-carrier concentration. This means that V_{oc} is determined by the relative rates at which electrons are injected from the photoexcited PMDPI to SnO_2 *vs.* depopulated from the SnO_2 *via* recombination. We assume the deposition of catalyst will not significantly alter the rate of electron injection from the excited PMPDI to the SnO_2 scaffolding. Thus, the V_{oc} values of nano-SnO_xC_y/PMPDI anodes without catalyst, with CoO_x added, and with Li-IrO_x added were compared to gain additional evidence for recombination in the present systems, Fig. 3.

Notably, we found an average V_{oc} of -0.07 ± 0.03 V *vs.* Ag/AgCl for nano-SnO_xC_y/PMPDI/Li-IrO_x anodes, a measurable improvement over the 0.00 ± 0.02 V *vs.* Ag/AgCl V_{oc} for anodes without the catalyst.[12] The negative, -70 ± 30 mV shift in V_{oc} of nano-SnO_xC_y/PMPDI/Li-IrO_x anodes relative to nano-SnO_xC_y/PMPDI anodes suggests a *ca.* 15-fold decrease in the rates of recombination relative to injection[12,44] *versus* the system with the CoO_x catalyst (see S4† for more details on how this 15-fold value was obtained). For comparison, the addition of CoO_x catalyst yields a *positive*[12] V_{oc} of $+0.05 \pm 0.02$ V *vs.* Ag/AgCl, consistent with an (undesired) increase in recombination in that CoO_x catalyst system.

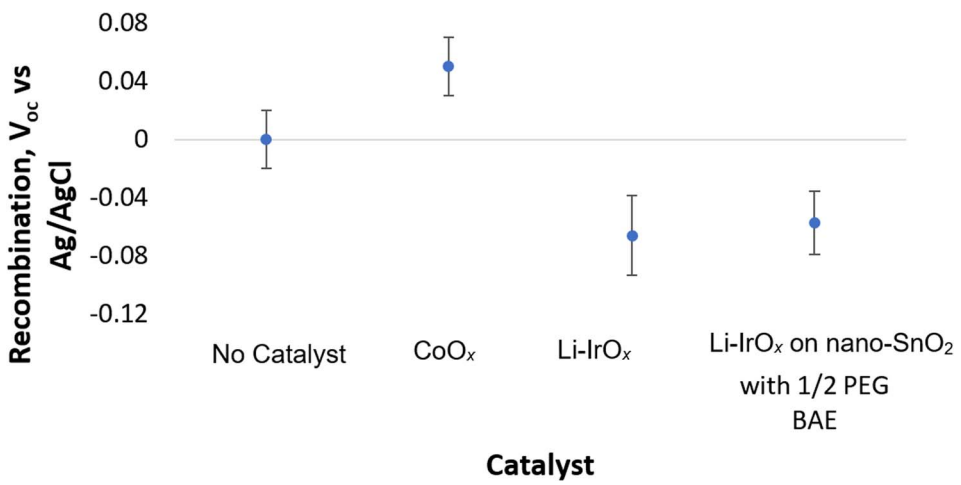

Fig. 3 V_{oc} *vs.* Ag/AgCl reference electrode in a half-cell setup for nano-SnO_xC_y/PMPDI anodes with differing catalyst addition. Note, no catalyst is added to the far-left data point. In this system, $V_{oc} \approx E_{F,n}$, the quasi-Fermi energy of electrons in the SnO_2 sub-bandgap states.[12,13]

Our first two of the five specific questions raised in the Introduction have been answered at this point: (1) yes, the kinetics of a WOC device can be altered by changing the WOCatalyst, such that undesirable kinetics pathways can be avoided through the use of a more effective catalyst; and (2) -1.2 mA cm^{-2} currents are achievable for H_2Q catalysis in a nano-SnO_xC_y/PMPDI/Li-IrO_x device.

Faradaic efficiencies for WOC

Often, photocurrent densities in DS-PECs are *assumed* to be entirely attributable to water oxidation catalysis. To avoid this unneeded assumption, we measured faradaic efficiencies for water oxidation catalysis with nano-SnO_xC_y/PMPDI/Li-IrO_x anodes using the established Generator–Collector method.[12,41] Faradaic efficiencies with Li-IrO_x were found to be 37 $\pm$ 10%, interestingly the same within error as the 31 $\pm$ 7% for anodes with CoO_x.[12] Hence, evidence for the expected at least modest improvement in selectivity for water-oxidation catalysis when using the Li-IrO_x WOCatalyst is not apparent within the stated error bars. However, the overall photocurrent is higher when using the Li-IrO_x WOCatalyst, so that more O_2 is in fact produced as expected when using Li-IrO_x rather than CoO_x as the WOCatalyst.

Testing the amount of recombination as a function of the amount of carbon

Nanostructured SnO_xC_y anodes were made deliberately containing *half* as much PEG-BAE organic stabilizer to test the effects of altering the amount of carbon trap states. Previously, with CoO_x, changing the amount of PEG-BAE added to nano-SnO_xC_y did change the amount of recombination observed.[33] However, herein, in anodes with Li-IrO_x catalyst, the degree of recombination in the halved PEG-BAE anodes as measured by V_{oc}, was found to be the same within error, as the nano-SnO_xC_y anodes made by the original synthesis, respectively -0.05 $\pm$ 0.02 V *vs.* Ag/AgCl and -0.07 $\pm$ 0.03 V *vs.* Ag/AgCl. These unchanged V_{oc} values within experimental error, despite halving the original many of C-containing stabilizer, suggests that Li-IrO_x is able to outcompete and overcome all the C-impurity based recombination in the nano-SnO_xC_y. Previously, this "1/2 as much carbon" test, while using the slower CoO_x catalyst, resulted in measurable differences in V_{oc}, and by implication recombination, again consistent with and supportive of a kinetics protection against at least C-impurity-based recombination when using the superior Li-IrO_x water-oxidation catalyst.[28]

As a visual representation of the kinetics of our system, intended as a working hypothesis for going forward, a scheme showing charge-transfer pathways in the nano-SnO_xC_y/PMPDI/Li-IrO_x system is shown in Scheme S1 of the ESI† for the interested reader.

A semi-quantitative comparison of the planar ALD-SnO_2 *vs.* the nanostructured SnO_xC_y systems: which is better?

To this point, we have shown that the employment of intrinsically superior WOCatalyst can outcompete the residual-carbon-related recombination, thus overcoming the anti-catalyst issue. In our previous report, we also have demonstrated that lowering carbon content in SnO_2 using ALD can improve the WOC performance. Here, a semi-quantitative comparison of the photoactivity of the lower-carbon-content ALD-SnO_2 planar system's performance compared to the higher-surface-area nano-SnO_xC_y system is carried out in order to quantitatively answer the question of "which system is fundamentally better at overcoming recombination attributed to residual carbon?".[46–50] Previously we have determined our synthesis of nano-SnO_xC_y to be approximately 11 $\pm$ 0.3 wt% carbon by XPS while the surface of the SnO_2 deposited by ALD is 5 $\pm$ 3 wt% carbon, and approximately 3 $\pm$ 3 wt% carbon after sputtering.[33]

Such a device comparison of the performance of the ALD-SnO_2 system *vs.* the nano-SnO_xC_y anodes requires a correction for their *ca.* two-order of magnitude different (*vide infra*) surface areas that results in a much lower photocurrent in the planar ALD-SnO_2 system. Additionally, different dye absorption in the ALD-SnO_2 *vs.* the nano-SnO_xC_y anode systems could be a factor that varies between the two anodes or catalyst deposition could change. Hence, we employed two methods that use a fundamentally different scientific basis to compare the two systems to mitigate assumptions that would significantly impact the conclusions, one based on (i) correcting the data for PMPDI absorbance, and a second method based on (ii) correcting for the electrochemically-active surface area.

Two methods for correcting for the different surface areas between the nano-SnO_xC_y system and the planar ALD-SnO_2 systems

Because of the significantly larger amount of surface area present in the nano-SnO_xC_y system *vs.* the planar ALD-SnO_2 system, considerably different dye optical absorption is observed. Indeed, saturation-dying of the planar and the nanostructured SnO_xC_y systems reveals a stark apparent difference between them, Fig. 4. In the first method, which corrects for the dye absorbance, Beer's Law was employed to calculate the ratio of dye on the planar ALD-SnO_2/PMPDI anode *vs.* the nanostructured nano-SnO_xC_y/PMPDI anode. As before, an approximately monolayer of dye was assumed[12,51] so as to obtain the PMPDI dye extinction coefficient used in the calculations. Using that extinction coefficient and Beer's Law on the optical absorption data, the ratio of dye absorbance at λ_{max}, after correction for SnO_2 absorbance, was found to be 1.0 : 94 for ALD-SnO_2/PMPD *vs.* nano-SnO_xC_y/PMPDI. Additional calculations determining the number of PMPDI dye molecules on both nano-SnO_xC_y/PMPDI and ALD-SnO_2/PMPDI anodes can be found in the ESI.†

Double-layer capacitance (C_d) was employed as a second means to differentiate and then compare the electrochemically active surface area of the two systems. By looking at the double-layer capacitance at a series of scan rates, a μF cm^{-2} scalar was determined (Fig. 5). This scalar was then used with the C_d of the nano-SnO_xC_y system to find the difference between the geometric and electrochemically-active surface area. This value can then be used with the geometric surface area of the nano-

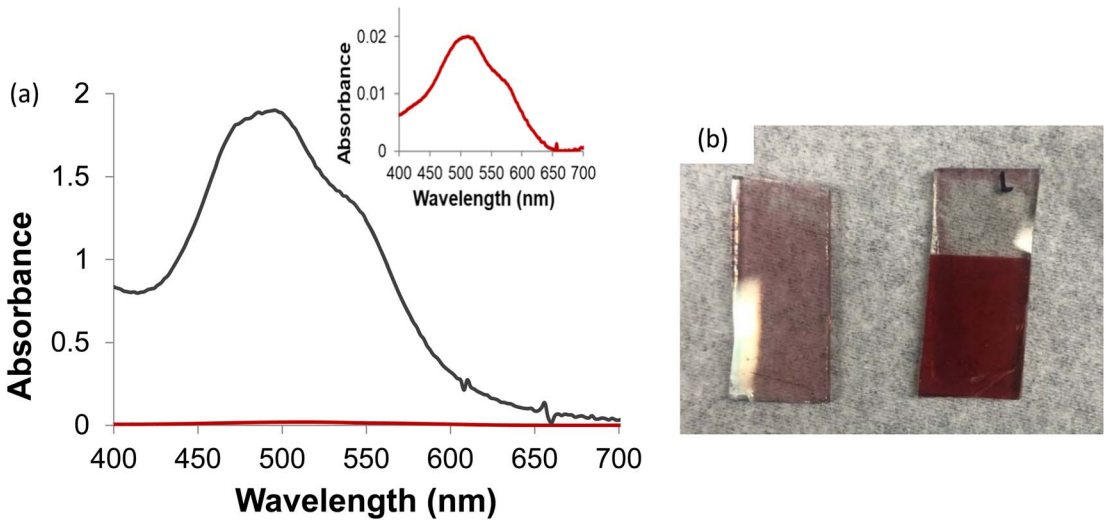

Fig. 4 (a) Optical absorbance spectrum of PMPDI on SnO_xC_y (black) and PMPDI on ALD-SnO_2 (red). Absorbance of bare SnO_2 film was subtracted off. The insert shows a zoomed-in plot of the absorbance of PMPDI on ALD-SnO_2. (b) Image of ALD-SnO_2/PMPDI anode (left) and nano-SnO_xC_y/PMPDI anode (right), where only the bottom two thirds of the anode is dyed.

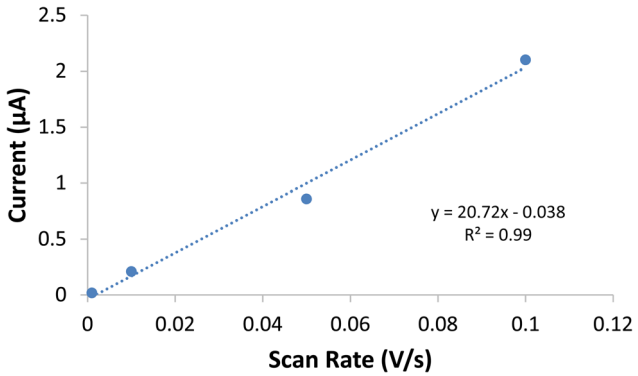

Fig. 5 Plot of scan rate *vs.* capacitive current for the ALD-SnO_2, where the slope of the line is directly proportional to the double layer capacitance.

SnO_xC_y anode tested in that particular experiment to find the electrochemically-active surface area of that anode. This method assumes the double-layer capacitance response is the same for the nano-SnO_xC_y and ALD-SnO_2. Using this determination, the ratio of electrochemically-active surface area for ALD-SnO_2 anodes *vs.* nano-SnO_xC_y anodes was found to be 1.0 : 190.

The different 1.0 : 94 and 1.0 : 190 values are, upon reflection, in reasonable (if not surprisingly good) agreement considering that the two methods measure a separate component of the system. The absorbance method looks at the PMPDI dye on dry anodes, while the capacitance method probes undyed anodes in solution (*i.e.*, examines them prior to dyeing) while those anodes are undergoing electrochemistry. Given that the two techniques are measuring different aspects of the (different) systems under two distinct sets of conditions, the factor of two between the values is better than expected. In any event, the values are more than sufficient for the purposes of the present study. Additionally, so as to not artificially over-enhance/overcorrect the current (*J*) data for the ALD-SnO_2 anodes, the corrections that follow deliberately emphasize the *smaller*, 1.0 : 94, value so as to *understate* the (corrected) current and implied conclusions. Moreover, control calculations are also provided in the ESI† using the other limit if the 1.0 : 190 correction to ensure that none of our conclusions change depending on which of the two possible surface-area corrections is used.

Results of comparing the Nano-SnO_xC_y system and the planar ALD-SnO_2 systems

To compare the different anodes, the above correction was made on photocurrent transient plots with the addition of H_2Q, Fig. 6. (The same data corrected using the higher electrochemically-active surface area value is provided as Fig. S3 of the ESI.†) The dashed lines represent a *hypothetical nano-structured (high surface area) reduced-carbon* version of the currently flat device.

Several observations are readily apparent from examining Fig. 6: first, the corrected ALD-SnO_2/PMPDI/CoO_x anodes (green trace) demonstrate the highest photocurrent of all the systems—a conclusion even more exaggerated if the larger 1.0 : 190 correction is used instead (Fig. S3 of the ESI†). Second, the nano-SnO_xC_y/PMPDI/CoO_x system is the worst performer (red trace). This conclusion, too, still holds with the larger correction (Fig. S3 of the ESI†). Third, the CoO_x-free systems nano-SnO_xC_y/PMPDI and ALD-SnO_2 (5 nm)/PMPDI perform essentially the same within experimental error (purple and blue curves, respectively). These results are consistent with and supportive of CoO_x yielding enhanced recombination resulting in the observed "anti-catalyst" effect. (This conclusion, too, is unchanged with the higher correction, although with that correction the lower-C ALD-SnO_2 (5 nm)/PMPDI system outperforms the greater C-containing nano-SnO_xC_y/PMPDI

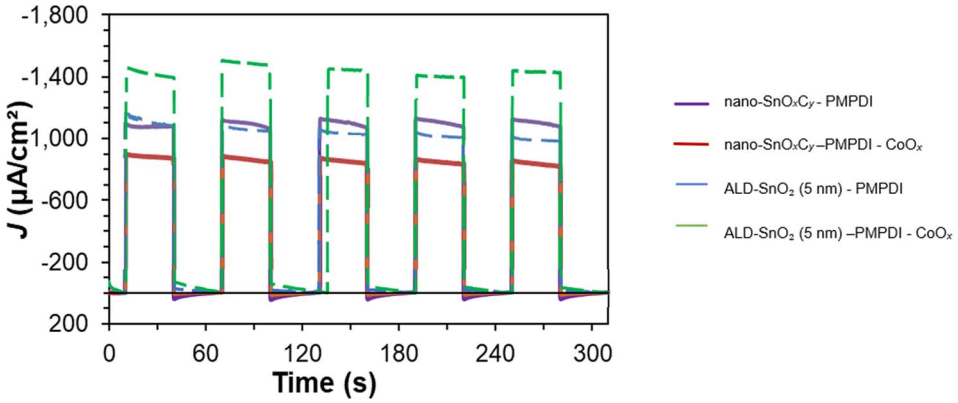

Fig. 6 $J-t$ transients in the presence of 20 mM H_2Q sacrificial reductant, with background dark current subtracted, at +0.2 V *vs.* Ag/AgCl in pH 7, 0.1 M KPi buffer with 30 s light/dark transients where purple is nano-SnO_xC_y/PMPDI, red is nano-SnO_xC_y/PMPDI/CoO_x, blue dashed is ALD-SnO_2(5 nm)/PMPDI (X94), and green dashed is ALD-SnO_2(5 nm)/PMPDI/CoO_x (X94). Both planar (blue and green) anodes are corrected (X94) to match the dye absorbance of the nanostructured anodes.

system. Evidence against diffusion limitations in the comparisons of the two systems are also presented in the ESI†). In other words, post scaling the ALD-SnO_2 anodes' current density and comparing that directly to the nano-SnO_xC_y system's current density, *the key finding is that the planar SnO_2 outperforms the nano-SnO_xC_y in terms of the current density*. Meriting noting here, however, is that the high-surface-area nano-SnO_xC_y anodes do produce more oxygen on a *per device basis* than their planar counterparts. This finding answers question 4 listed in the Introduction, demonstrating that lower-carbon ALD-SnO_2 produces anodes that outperform their nano-SnO_2 anode counterpart systems, on both per amount of dye and per electrochemically-active surface area basis[13] at potentials over +0.6 V *vs.* Ag/AgCl.

Perhaps most important are the steady-state photocurrents post the addition of CoO_x catalyst: the ALD-SnO_2 anodes show a *ca.* 44% *increase* in photocurrent in comparison to the nano-SnO_xC_y anodes that exhibit a *ca.* 24% *decrease* in photocurrent. This net 68% reversal of the "anti-catalyst" effect in anodes with less carbon impurity *makes apparent that decreasing the amount of carbon by using ALD is a successful strategy en route to better performing anodes*. This conclusion is further supported by the V_{oc} values observed in the ALD-SnO_2 system: ALD-SnO_2 anodes coated in PMPDI were found to have a V_{oc} of -0.03 ± 0.03 and to be the same within error, -0.03 ± 0.04, with the addition of the CoO_x catalyst. This ALD-SnO_2 strategy is of particular interest as it demonstrates a rare-element-free method of overcoming the issue of residual carbon dominated recombination without altering the WOCatalyst. With the ALD-SnO_2(5 nm)/PMPDI/CoO_x anodes, photocurrent densities are comparable to those seen in the nano-SnO_xC_y/PMPDI/Li-IrO_x anodes on a per-dye or per-electrochemically-active-surface-area basis, without the use of iridium. Hence, if this level of photocurrent density can be achieved using a more carbon-free nano-SnO_2 preparation, then in principle the use of a rare-element catalyst can be avoided while still achieving the higher photocurrent. It follows that studies aimed at the preparation of low-carbon, organic-stabilizer-free nano-SnO_2 syntheses are, therefore, of considerable interest.

Finally, provided in Fig. S4 of the ESI,† is a comparison of photocurrents between the anodes described herein and the previously studied best performing nano-SnO_xC_y/PMPDI/PMPDI/AlO_n (0.6 nm, 85 °C deposition)/CoO_x anodes which added an additional alumina overlayer by ALD.[13] When corrected for absorbance, the anodes made using planar SnO_2 deposited by ALD were shown to have a higher photocurrent compared to the previous best nano-SnO_xC_y/PMPDI/AlO_n (0.6 nm, 85 °C deposition)[13] systems at potentials over +0.6 V *vs.* Ag/AgCl. In short, it is clear that using a more phase-pure ALD-SnO_2 is a viable strategy to avoid the undesired recombination effects of residual carbon issue in metal-oxides such as nano-SnO_xC_y. In addition, designing a *carbon-free nano-SnO_x synthesis* that uses both aspects of the work herein—lowering the amount of carbon in the SnO_2, while maintaining the high surface area—is a recommended direction of future research based on the findings in the present study.

Combining planar ALD-SnO_2 and Li-IrO_x catalyst in one, best-to-date, device

In order to study a best possible device in terms of its efficiency and address question 5 listed in the Introduction, the two methods detailed above were combined and tested together for water oxidation catalysis, specifically altering the WOCatalyst to the state-of-the-art Li-IrO_x while also using lower-carbon ALD-SnO_2. Photocurrent data for anodes in H_2Q were measured for ALD-SnO_2 anodes without catalyst, with CoO_x, and with Li-IrO_x (Fig. 7).

Anodes with Li-IrO_x catalyst again yield an increase in photocurrents of approximately 4-times with the WOCatalyst addition in the ALD-SnO_2 system, resulting in significantly higher photocurrents than their counterparts with CoO_x catalyst. Combining both methods of overcoming carbon-based recombination in the anode results in the most photoactive device by far on a per-dye or a per-electrochemically-active-surface-area basis, outperforming the ALD-SnO_2/PMPDI/CoO_x anodes, which themselves outperform their nano-SnO_xC_y

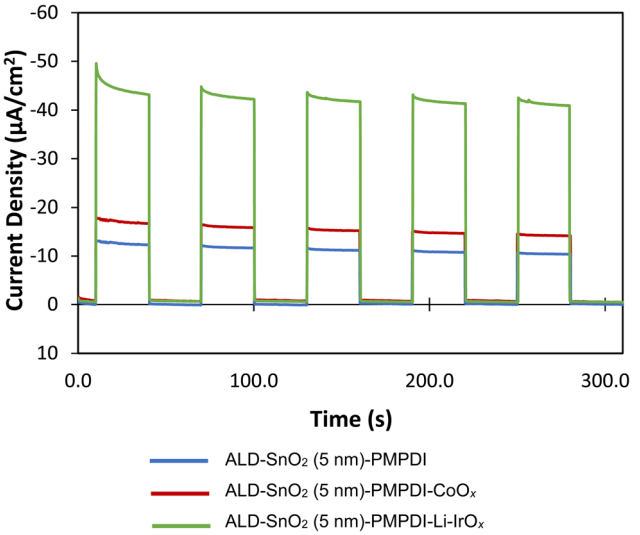

Fig. 7 $J-t$ transients in the presence of 20 mM H_2Q sacrificial reductant, with background dark current subtracted, at +0.2 V *vs.* Ag/AgCl in pH 7, 0.1 M KPi buffer with 30 s light/dark transients where blue is ALD-SnO_2(5 nm)/PMPDI, red is ALD-SnO_2(5 nm)/PMPDI/CoO_x, and green is ALD-SnO_2(5 nm)/PMPDI/Li-IrO_x (green) anodes.

counterparts. Similar, albeit significantly lower, results can be seen on ALD-SnO_2 anode systems without H_2Q with and without Li-IrO_x, Fig. S5.†

The V_{oc} was measured for the ALD-SnO_2/PMPDI/Li-IrO_x anodes in order to probe recombination in this combined system. The anodes exhibit a V_{oc} of -0.09 ± 0.03 V *vs.* Ag/AgCl, the same value within error as both the nano-SnO_xC_y/PMPDI/Li-IrO_x and the nano-SnO_xC_y/PMPDI/Li-IrO_x anodes made with nano-SnO_xC_y containing half as much PEG-BAE organic stabilizer. These V_{oc} values support our finding that the improved Li-IrO_x catalyst by itself can overcome recombination in our devices attributable to residual carbon.

Lastly, the faradaic efficiency for water oxidation was also tested for the ALD-SnO_2/PMPDI/Li-IrO_x anodes resulting in an efficiency of 60 ± 11% for water oxidation. This faradaic efficiency is increased over the 37 ± 10% detailed above for nano-SnO_xC_y/PMPDI/Li-IrO_x anodes. This increase in faradaic efficiency over the nano-SnO_xC_y/PMPDI/Li-IrO_x anodes implies that more of the photocurrent generated is originating from oxygen generation, rather than peroxide formation or other side reactions. The increased faradaic efficiency is furthermore consistent with the increase we previously observed when comparing faradaic efficiencies for nano-SnO_xC_y/PMPDI/CoO_x to that for ALD-SnO_2/PMPDI/CoO_x, 31 ± 7% and 45 ± 6%, respectively.[12,33]

Conclusions

The photoelectrochemical WOC research presented investigates the impact on photocurrent of changing the WOCatalyst, specifically the decrease in current due to carbon impurity-based recombination. We were able to answer the five specific questions posed at the beginning of the study: (1) *yes*, improving the WOCatalyst to the state-of-the-art Li-IrO_x WOCatalyst that is the best-in-class alters the charge transfer kinetics to outcompete recombination pathways attributable to residual carbon. More specifically, the use of a Li-IrO_x WOCatalyst yielded the desired *increase* in photocurrent upon catalyst addition, thereby overcoming the decrease in photocurrent and anti-catalyst effect seen with the slower, earth-abundant CoO_x WOCatalyst. We also found (2) that the maximum steady-state current from such simple organic-dye-based devices, nano-SnO_xC_y/PMPDI/Li-IrO_x produced -42 μA cm^{-2} at +0.4 V *vs.* Ag/AgCl for water oxidation (and -1.2 mA cm^{-2} photocurrent for H_2Q catalysis). Additionally (3), dye adsorption and double-layer capacitance were studied and used to semi-quantitatively compare the two systems, from which we found the interesting result that (4) *the simple, planar ALD-SnO_2 system* is more efficient than the FTO/nano-SnO_xC_y/PMPDI/CoO_x system, once the ≥*ca.* 10^2 different surface area of the two systems is taken into account. Lastly, (5) a device made using the *combination* of ALD-SnO_2 and the superior Li-IrO_x catalyst was shown to have the highest photoactivity on a per-dye or a per-electrochemically-active-surface-area basis, higher than both anodes made using only one of the two strategies described above. That achievement so noted, had we started with Li-IrO_x as the WOCatalyst initially in 2017, we likely would have never discovered the role carbon plays when employing nano-SnO_xC_y, as we would have never observed the tell-tale anti-catalyst effect.

Some needed directions of future research are apparent from the present studied. One is that the development of an earth-abundant WOCatalyst that is more selective for water oxidation's $4e^-$ process over the $2e^-$ peroxide reaction remains very desirable. Second, fast spectroscopic kinetic and mechanistic studies aimed at verifying or refuting the individual charge-transfer pathways proposed in Scheme S1† as a working hypothesis would also be most welcome. Finally, the development of an *organic stabilizer-free, low-carbon nano-SnO_2 synthesis* is a high priority that promises to be important to all areas in materials chemistry and science currently employing nano-SnO_xC_y. In short, DS-PECs for WOC and the areas they depend on continue to be interesting as well as promising areas with many directions of research meriting additional research.

Conflicts of interest

There are no conflicts to declare.

Acknowledgements

This research was supported by the National Science Foundation under Grant No. 1664646. The authors thank the members of Prof. Finke's research group for reading draft versions of this manuscript and providing valuable feedback. We also thank the Analytical Research Core at Colorado State University for instrument access and assistance. This research used the Materials Synthesis and Characterization Facility of the Center for Functional Nanomaterials, which is a U.S. Department of Energy Office of Science User Facility, at Brookhaven National Laboratory under Contract No. DE-SC0012704.

References

1 J. T. Kirner and R. G. Finke, Water-Oxidation Photoanodes Using Organic Light- Harvesting Materials: A Review, *J. Mater. Chem. A*, 2017, **5**, 19560–19592.
2 A. J. Bard and M. A. Fox, Artificial Photosynthesis: Solar Splitting of Water to Hydrogen and Oxygen Water Splitting, *Acc. Chem. Res.*, 1995, **28**, 141–145.
3 R. E. Smalley, Future Global Energy Prosperity: The Terawatt Challenge, *Materials Matters*, 2004, **30**, 412–417.
4 N. S. Lewis and D. G. Nocera, Powering the Planet: Chemical Challenges in Solar Energy Utilization, *Proc. Natl. Acad. Sci. USA*, 2006, **103**, 15729–15735.
5 L. Steier and S. Holliday, A Bright Outlook on Organic Photoelectrochemical Cells for Water Splitting, *J. Mater. Chem. A*, 2018, **6**, 21809–21826.
6 D. Wang, Z. Xu, M. v. Sheridan, J. J. Concepcion, F. Li, T. Lian and T. J. Meyer, Photodriven Water Oxidation Initiated by a Surface Bound Chromophore-Donor-Catalyst Assembly, *Chem. Sci.*, 2021, **12**, 14441–14450.
7 S. Yun, N. Vlachopoulos, A. Qurashi, S. Ahmad and A. Hagfeldt, Dye Sensitized Photoelectrolysis Cells, *Chem. Soc. Rev.*, 2019, **48**, 3705–3722.
8 M. Bonchio, Z. Syrgiannis, M. Burian, N. Marino, E. Pizzolato, K. Dirian, F. Rigodanza, G. A. Volpato, G. la Ganga, N. Demitri, S. Berardi, H. Amenitsch, D. M. Guldi, S. Caramori, C. A. Bignozzi, A. Sartorel and M. Prato, Hierarchical Organization of Perylene Bisimides and Polyoxometalates for Photo-Assisted Water Oxidation, *Nat. Chem.*, 2018, **11**, 146–153.
9 A. Mishra, M. K. R. Fischer and P. Büuerle, Metal-Free Organic Dyes for Dye-Sensitized Solar Cells: From Structure: Property Relationships to Design Rules, *Angew. Chem., Int. Ed.*, 2009, **48**, 2474–2499.
10 D. P. Hagberg, T. Marinado, K. M. Karlsson, K. Nonomura, P. Qin, G. Boschloo, T. Brinck, A. Hagfeldt and L. Sun, Tuning the HOMO and LUMO Energy Levels of Organic Chromophores for Dye Sensitized Solar Cells, *J. Org. Chem.*, 2007, **72**, 9550–9556.
11 J. T. Kirner, J. J. Stracke, B. A. Gregg and R. G. Finke, Visible-Light-Assisted Photoelectrochemical Water Oxidation by Thin Films of a Phosphonate-Functionalized Perylene Diimide Plus CoO_x Cocatalyst, *ACS Appl. Mater. Interfaces*, 2014, **6**, 13367–13377.
12 J. T. Kirner and R. G. Finke, Sensitization of Nanocrystalline Metal Oxides with a Phosphonate-Functionalized Perylene Diimide for Photoelectrochemical Water Oxidation with a CoO_x Catalyst, *ACS Appl. Mater. Interfaces*, 2017, **9**, 27625–27637.
13 C. F. Jewell, A. Subramanian, C.-Y. Nam and R. G. Finke, Ultrathin Alumina Passivation for Improved Photoelectrochemical Water Oxidation Catalysis of Tin Oxide Sensitized by a Phosphonate-Functionalized Perylene Diimide First without, and Then with, CoO_y, *Sustainable Energy Fuels*, 2021, **5**, 5257–5269.
14 F. Liu, J. J. Concepcion, J. W. Jurss, T. Cardolaccia, J. L. Templeton and T. J. Meyer, Mechanisms of Water Oxidation from the Blue Dimer to Photosystem II, *Inorg. Chem.*, 2008, **47**, 1727–1752.
15 T. G. Ulusoy Ghobadi, A. Ghobadi, M. Buyuktemiz, E. A. Yildiz, D. Berna Yildiz, H. G. Yaglioglu, Y. Dede, E. Ozbay and F. Karadas, A Robust, Precious-Metal-Free Dye-Sensitized Photoanode for Water Oxidation: A Nanosecond-Long Excited-State Lifetime through a Prussian Blue Analogue, *Angew. Chem.*, 2020, **132**, 4111–4119.
16 Z. Deng, H. W. Tseng, R. Zong, D. Wang and R. Thummel, Preparation and Study of a Family of Dinuclear Ru(II) Complexes That Catalyze the Decomposition of Water, *Inorg. Chem.*, 2008, **47**, 1835–1848.
17 Y. v. Geletii, C. Besson, Y. Hou, Q. Yin, D. G. Musaev, D. Quiñ, R. Cao, K. I. Hardcastle, A. Proust, P. Kö and C. L. Hill, Structural, Physicochemical, and Reactivity Properties of an All-Inorganic, Highly Active Tetraruthenium Homogeneous Catalyst for Water Oxidation, *J. Am. Chem. Soc.*, 2009, **131**, 17360–17370.
18 M. Yamamoto, L. Wang, F. Li, T. Fukushima, K. Tanaka, L. Sun and H. Imahori, Visible Light-Driven Water Oxidation Using a Covalently-Linked Molecular Catalyst–Sensitizer Dyad Assembled on a TiO_2 Electrode, *Chem. Sci.*, 2016, **7**, 1430–1439.
19 M. Yamamoto, Y. Nishizawa, P. Chá, F. Li, T. Rn Pascher, V. Sundströ, L. Sun and H. Imahori, Visible Light-Driven Water Oxidation with a Subporphyrin Sensitizer and a Water Oxidation Catalyst, *Chem. Commun.*, 2016, **52**, 13702–13705.
20 F. Li, K. Fan, B. Xu, E. Gabrielsson, Q. Daniel, L. Li and L. Sun, Organic Dye-Sensitized Tandem Photoelectrochemical Cell for Light Driven Total Water Splitting, *J. Am. Chem. Soc.*, 2015, **137**, 9153–9159.
21 K.-R. Wee, B. D. Sherman, M. K. Brennaman, M. v. Sheridan, A. Nayak, L. Alibabaei and T. J. Meyer, An Aqueous, Organic Dye Derivatized SnO_2/TiO_2 Core/Shell Photoanode, *J. Mater. Chem. A*, 2016, **4**, 2969–2975.
22 G. F. Moore, J. D. Blakemore, R. L. Milot, J. F. Hull, H.-E. Song, L. Cai, C. A. Schmuttenmaer, R. H. Crabtree and G. W. Brudvig, A Visible Light Water-Splitting Cell with a Photoanode Formed by Codeposition of a High-Potential Porphyrin and an Iridium Water-Oxidation Catalyst, *Energy Environ. Sci.*, 2011, **4**, 2389–2392.
23 J. R. Swierk, D. D. Méndez-Hernádez, N. S. Mccool, P. Liddell, Y. Terazono, I. Pahk, J. J. Tomlin, N. v Oster, T. A. Moore, A. L. Moore, D. Gust, T. E. Mallouk and D. D. Méndez-Hernández, Metal-Free Organic Sensitizers for Use in Water- Splitting Dye-Sensitized Photoelectrochemical Cells, *Proc. Natl. Acad. Sci. USA*, 2015, **112**, 1681–1686.
24 F. Ronconi, Z. Syrgiannis, A. Bonasera, M. Prato, R. Argazzi, S. Caramori, V. Cristino and C. A. Bignozzi, Modification of Nanocrystalline WO_3 with a Dicationic Perylene Bisimide: Applications to Molecular Level Solar Water Splitting, *J. Am. Chem. Soc.*, 2015, **137**, 4630–4633.

25 R. J. Kamire, K. L. Materna, W. L. Hoffeditz, B. T. Phelan, J. M. Thomsen, O. K. Farha, J. T. Hupp, G. W. Brudvig and M. R. Wasielewski, Photodriven Oxidation of Surface-Bound Iridium-Based Molecular Water-Oxidation Catalysts on Perylene-3,4-Dicarboximide-Sensitized TiO_2 Electrodes Protected by an Al_2O_3 Layer, *J. Phys. Chem. C*, 2017, **121**, 3752–3764.

26 M. Bledowski, L. Wang, A. Ramakrishnan, O. v. Khavryuchenko, V. D. Khavryuchenko, P. C. Ricci, J. Strunk, T. Cremer, C. Kolbeck and R. Beranek, Visible-Light Photocurrent Response of TiO_2–Polyheptazine Hybrids: Evidence for Interfacial Charge-Transfer Absorption, *Phys. Chem. Chem. Phys.*, 2011, **13**, 21511–21519.

27 Y. Liu, X. Liang, H. Chen, R. Gao, L. Shi, L. Yang and X. Zou, Iridium-Containing Water-Oxidation Catalysts in Acidic Electrolyte, *Chin. J. Catal.*, 2021, **42**, 1054–1077.

28 G. Hu, J. L. Troiano, U. T. Tayvah, L. S. Sharninghausen, S. B. Sinha, Y. Shopov, B. Q. Mercado, R. H. Crabtree and G. W. Brudvig, Accessing Molecular Dimeric Ir Water Oxidation Catalysts from Coordination Precursors, *Inorg. Chem.*, 2021, **60**, 14349–14356.

29 H. H. Cho, L. Yao, J. H. Yum, Y. Liu, F. Boudoire, R. A. Wells, N. Guijarro, A. Sekar and K. Sivula, A Semiconducting Polymer Bulk Heterojunction Photoanode for Solar Water Oxidation, *Nat. Catal.*, 2021, **4**, 431–438.

30 M. S. Eberhart, D. Wang, R. N. Sampaio, S. L. Marquard, B. Shan, M. K. Brennaman, G. J. Meyer, C. Dares and T. J. Meyer, Water Photo-Oxidation Initiated by Surface-Bound Organic Chromophores, *J. Am. Chem. Soc.*, 2017, **139**, 16248–16255.

31 T. Gobbato, F. Rigodanza, E. Benazzi, P. Costa, M. Garrido, A. Sartorel, M. Prato and M. Bonchio, Enhancing Oxygenic Photosynthesis by Cross-Linked Perylenebisimide "Quantasomes, *J. Am. Chem. Soc.*, 2022, **144**, 14021–14025.

32 Y. Zhu, D. Wang, W. Ni, G. G. Gurzadyan, L. Sun, T. J. Meyer and F. Li, Water Oxidation by a Noble Metal-Free Photoanode Modified with an Organic Dye and a Molecular Cobalt Catalyst, *J. Mater. Chem. A*, 2022, **10**, 9121–9128.

33 C. F. Jewell, A. Subramanian, C.-Y. Nam and R. G. Finke, Understanding the "Anti-Catalyst" Effect with Added CoO_x Water Oxidation Catalyst in Dye-Sensitized Photoelectrolysis Cells: Carbon Impurities in Nanostructured SnO_2 Are the Culprit, *ACS Appl. Mater. Interfaces*, 2022, **14**, 25326–25336.

34 I. Neelakanta Reddy, B. Akkinepally, N. Siva Kumar, M. Asif, J. Shim and C. Bai, SnO_2 Nanoparticles Anchored on Carbon Spheres for Enhanced Charge Generation and Potentiodynamic Effects, *J. Electroanal. Chem.*, 2023, **937**, 117411.

35 J. Gao, C.-Q. Xu, S.-F. Hung, W. Liu, W. Cai, Z. Zeng, C. Jia, H. Ming Chen, H. Xiao, J. Li, Y. Huang and B. Liu, Breaking Long-Range Order in Iridium Oxide by Alkali Ion for Efficient Water Oxidation, *J. Am. Chem. Soc.*, 2019, **141**, 3014–3023.

36 B. J. Brennan, A. C. Durrell, M. Koepf, R. H. Crabtree and G. W. Brudvig, Towards Multielectron Photocatalysis: A Porphyrin Array for Lateral Hole Transfer and Capture on a Metal Oxide Surface, *Phys. Chem. Chem. Phys.*, 2015, **17**, 12728–12734.

37 S. Evans, Correction for the Effects of Adventitious Carbon Overlayers in Quantitative XPS Analysis, *Surf. Interface Anal.*, 1997, **25**, 924–930.

38 G. Greczynski and L. Hultman, X-Ray Photoelectron Spectroscopy: Towards Reliable Binding Energy Referencing, *Prog. Mater. Sci.*, 2020, **107**, 100591.

39 Y. Zhao, J. R. Swierk, J. D. Megiatto Jr, B. Sherman, W. J. Youngblood, D. Qin, D. M. Lentz, A. L. Moore, T. A. Moore, D. Gust, T. E. Mallouk and T. J. Meyer, Improving the Efficiency of Water Splitting in Dye-Sensitized Solar Cells by Using a Biomimetic Electron Transfer Mediator, *Proc. Natl. Acad. Sci. USA*, 2012, **109**, 15612–15616.

40 D. L. Ashford, B. D. Sherman, R. A. Binstead, J. L. Templeton and T. J. Meyer, Electro-Assembly of a Chromophore-Catalyst Bilayer for Water Oxidation and Photocatalytic Water Splitting, *Angew. Chem., Int. Ed.*, 2015, **54**, 4778–4781.

41 B. D. Sherman, M. v Sheridan, C. J. Dares and T. J. Meyer, Two Electrode Collector−Generator Method for the Detection of Electrochemically or Photoelectrochemically Produced O_2, *Anal. Chem.*, 2016, **88**, 7076–7082.

42 It is important to note here that a comparison of the catalysts based on the number of active sites or amount of catalyst deposited would be ideal, but is not yet possible as the amount of catalyst deposited, much less the number of active sites, is not known.

43 One alternative hypothesis that needs to be noted is that because Li-IrO_x is spray-deposited using a nebulizer and CoO_x is photoelectrochemically deposited, possibly preferentially onto the electrically conductive carbon impurities, it is conceivable that electrodepositing Li-IrO_x could result in further preferential deposition onto carbon impurities, but this is not experimentally feasible herein. Another alternative hypothesis is that spray depositing the Li-IrO_x catalyst could passivate the carbon-based recombination sites.

44 S. Ardo and G. J. Meyer, Photodriven Heterogeneous Charge Transfer with Transition-Metal Compounds Anchored to TiO_2 Semiconductor Surfaces, *Chem. Soc. Rev.*, 2009, **38**, 115–164.

45 J. R. Swierk, N. S. McCool, T. P. Saunders, G. D. Barber, M. E. Strayer, N. M. Vargas-Barbosa and T. E. Mallouk, Photovoltage Effects of Sintered IrO_2 Nanoparticle Catalysts in Water-Splitting Dye-Sensitized Photoelectrochemical Cells, *J. Phys. Chem. C*, 2014, **118**, 17046–17053.

46 H. Y. Kim, J. H. Nam, S. M. George, J. S. Park, B. K. Park, G. H. Kim, D. J. Jeon, T. M. Chung and J. H. Han, Phase-Controlled SnO_2 and SnO Growth by Atomic Layer Deposition Using Bis(N-Ethoxy-2,2-Dimethyl Propanamido) Tin Precursor, *Ceram. Int.*, 2019, **45**, 5124–5132.

47 J. Sundqvist, J. Lu, M. Ottosson and A. Hårsta, Growth of SnO_2 Thin Films by Atomic Layer Deposition and

Chemical Vapour Deposition: A Comparative Study, *Thin Solid Films*, 2006, **514**, 63–68.
48 M. N. Mullings, C. Hägglund and S. F. Bent, Tin Oxide Atomic Layer Deposition from Tetrakis(Dimethylamino)Tin and Water, *J. Vac. Sci. Technol., A*, 2013, **31**, 061503.
49 J. Heo, A. S. Hock and R. G. Gordon, Low Temperature Atomic Layer Deposition of Tin Oxide, *Chem. Mater.*, 2010, **22**, 4964–4973.
50 H. E. Cheng, D. C. Tian and K. C. Huang, Properties of SnO_2 Films Grown by Atomic Layer Deposition, *Procedia Eng.*, 2012, **36**, 510–515.
51 I. Ichinose, H. Senzu and T. Kunitake, Stepwise Adsorption of Metal Alkoxides on Hydrolyzed Surfaces: A Surface Sol-Gel Process, *Chem. Lett.*, 1996, **25**, 831–832.